RSC Advances

# Growth of SnO2 nanowire arrays by ultrasonic spray pyrolysis and their gas sensing performance


| | |
|---|---|
| Journal: | *RSC Advances* |
| Manuscript ID: | RA-ART-06-2014-005682.R1 |
| Article Type: | Paper |
| Date Submitted by the Author: | 09-Aug-2014 |



| | |
|---|---|
| Complete List of Authors: | Sun, Jianbo; Harbin Normal University, School of Physics and Electronic Engineering<br>Sun, Peng; Jilin University, College of Electronic Science and Engineering<br>Zhang, Dalin; Jilin University, College of Electronic Science and Engineering<br>Xu, Jing; Jilin University, College of Electronic Science and Engineering<br>Liang, Xishuang; Jilin University, College of Electronic Science and Engineering<br>Liu, Fengmin; Jilin University, College of Electronic Science and Engineering<br>lu, geyu; jilin university, EE |

# Growth of $SnO_2$ nanowire arrays by ultrasonic spray pyrolysis and their gas sensing performance

*Jianbo Sun[1],Peng Sun[2], Dalin Zhang[2], Jing Xu[2], Xishuang Liang[2],Fengmin Liu[2]*,*

*Geyu Lu[2]**

1.Key Laboratory for Photonic and Electronic Bandgap Materials, Ministry of Education, School of Physics and Electronic Engineering, Harbin Normal University, Harbin 150025, P. R. China.

2.State Key Laboratory on Integrated Optoelectronics Jilin University Region; College of Electronic Science and Engineering, Jilin University, 2699 Qianjin Street, Changchun 130012, P. R. China

Corresponding author. Tel.: +86-431-85167808; Fax: +86-431-85167808.

E-mail Address: liufm@jlu.edu.cn

lugy@jlu.edu.cn

**Abstract**

We demonstate direct synthesis of $SnO_2$ nanowire arrays on a glass substrate by using a ultrasonic spray pyrolysis method combined with sintering. The obtained products are characterized by the X-ray diffraction (XRD), the scan electron microscopy (SEM), the transmission electron microscopy (TEM) and the high resolution TEM. The results show that the $SnO_2$ nanowire arrays consist of single crystalline nanowires with a diameter of 50-70 nm and a length of 5-7 μm. There are two different nanowire growth directions due to the oxygen defect growth. The growth mechanism for the formation of $SnO_2$ nanowire arrays is investigated. We fabricated a platform gas sensor based on the $SnO_2$ nanowire arrays. The sensor exhibits better sensitivity and selectivity to $NO_2$ than that based on $SnO_2$ nanoparticles. The gas sensing mechanism is also discussed.

**Introduction**

One-dimensional (1D) nanostructures materials have received much attention due to their special properties and applied potential, since the discovery of carbon nanotubes in the last century. Nanorod, nanowires, nanotubes, nanocables, and nanofibers have been extensively reported [1-6]. Arrays of vertically aligned nanostructures like nanowires and nanotubes have been found to have advantage of high specific area and fast electron transport. These properties normally increase the gas sensing performance of semiconductor materials [7,8].

$SnO_2$ is a significant wide band-gap semiconductor with high chemical stability and good optical, electrical and mechanical properties [9]. It has been widely applied in various fields like gas sensors, transparent conducting electrodes and dye-sensitized solar cells [10-12]. In recent years, the synthesis of $SnO_2$ one-dimensional structure widely reported. Normal synthesis methods include thermal evaporation [13], laser ablation [14], solution phase growth [15], chemical vapor deposition (CVD) [16], electrostatic spinning [17], electron-beam lithography (EBL) [18]. These methods are affected by extreme conditions and complicated procedures.

As one of the conventional deposition techniques, the Ultrasonic spray pyrolysis (USP) method has been used to produce various nanostructures. The USP has advantages like low cost, minimal experimental apparatus and offers a great flexibility in a continuous flow process for the synthesis of oxide materials. To our best knowledge, there are few reports about the synthesis of $SnO_2$ nanowire arrays using the USP.

In this study, we use the USP method combining with sintering to synthesize $SnO_2$ nanowire arrays. The effect of time and temperature is investigated and a possible mechanism of nanowire growth and assembly is proposed. The gas sensing properties of $SnO_2$ nanowire arrays to various gases are studied. The material shows a good response to $NO_2$.

**Experimental details**

*1.1 Synthesis of $SnO_2$ nanowires array using the USP system*

A schematic diagram of the ultrasonic spray pyrolysis (USP) system is shown in Fig 1a. The USP system is mainly composed of three parts. The first part has an aerosol generator and a flow controller. The atomized reactant generates by using an ultrasonic transducer (medical ultrasonic generator, YUYUE AI-502; ultrasonic frequency: 1.7 MHz, rate of atomization: 2.2 ml/hour). High purity nitrogen is used as the carrier gas. The gas flow rate is controlled by a flow controller (300 sccm-1000 sccm). The second part is the reaction zone which contains a sealed quartz tube and a heater (tubular sintering furnace, the error range of temperature is within 5 $^{o}$C). The third

part is a conical flask to collect the residues from the reaction zone.

Laboratory chemicals and reagents used in the analytical grade were purchased from the Sinopharm Chemical Reagents Co., China. There was no further purification processing. The practical operations were presented as follows. A prepared 10 ml aqueous solution of $SnCl_4 \cdot 5H_2O$ (3.54 g) was stirred for 20 min, and then 0.5 ml of 0.2 mol/L hydrochloric acid solution was dropped into the flask to form a homogeneous solution.

The diameter of nebulized droplets was calculated to be 3 μm by Equation (1). Here, α is constant (for $SnCl_4$ solution, α is 0.34). What's more, σ stands for liquid surface tension (0.0859N/m); ρ is liquid density(about 1.16g/ml, at 25℃); f is the ultrasonic frequency (1.7 MHz).

$$D = \alpha\left(\frac{8 \bullet \pi \bullet \sigma}{\rho \bullet f^2}\right)^{\frac{1}{3}} \quad (1)$$

The precursor solution was then transferred into an ultrasonic transducer and changed to aerosol. The aerosol was sent into the reaction zone by the $N_2$ carrier gas (500 sccm). The quartz substrates (5.5 mm*5.5 mm*0.5 mm) were placed in the reaction zone. The temperature in the reaction zone was 400 $^oC$ measured by a thermocouple. The reaction lasts for 2 hours at this temperature. The aerosol forms single-crystalline $SnO_2$ nanowires arrays on the quartz substrate through heating, solvent evaporation, and pyrolysis. The $SnO_2$ nanowires arrays were sintered for 2 hours at 500 $^oC$.

*1.2 Characterizations*

The X-ray diffraction (XRD) pattern was recorded with a Rigaku D/max-2500 diffractometer with Cu-Ka radiation (λ=1.5418 Å) in the range of 20-80$^o$. Filed-emission scanning electron microscopy (FESEM) observations were performed with a JEOL JSM-7500F microscope, operated at an acceleration voltage of 15 kV. Transmission electron microscopy (TEM) and high-resolution transmission electron microscopy (HRTEM) measurements were obtained on a JEOL JEM-2100 microscope operated at 200 kV. Thermogravimetric (TG) analysis and differential scanning calorimetric (DSC) measurements were carried out using a NETZSCH STA 449F3 simultaneous thermo-gravimetric analyzer under air in the temperature range from 30 to 800 $^oC$ with a heating rate of 10 $^oC$ /min.

*1.3 Gas sensing experiments*

Gas sensing properties of as-produced $SnO_2$ nanowires arrays were performed through a static state testing system. As described above, the $SnO_2$ nanowires were formed on the square quartz substrate by the USP method. The structure of sensors are presented in Fig. 1b. The copper electrodes on the substrate were mounted by copper wire on phenolic resin socket. An integrated Pt heater was also printed on the back of the quartz substrate. The sensors based on $SnO_2$ nanowires were measured by the static system (Fig.S1), which contains an air chamber (volume 50L) and a data analyzing system. The sensor was placed in the air chamber, and its resistance change was monitored by a multimeter (FLUK 8846A). The temperature and humidity in air chamber were controlled to be 25 $^oC$ and 10% RH. The response of the sensor was defined as Rg/Ra; with Ra and Rg being the resistances of the sensor in the target gas and air, respectively.

**Results**

1D $SnO_2$ nanowires arrays were obtained by sintering for 2 hours at 500 $^oC$. Figure 2 shows the X-ray diffraction (XRD) results of the synthesized $SnO_2$ nanowires arrays. All diffraction peaks can be indexed to the rutile phase of $SnO_2$ . The $SnO_2$ lattice constants obtained by

refinement of the XRD data of the nanowires are a = 4.7382 and c = 3.1871, which are consistent with those of the bulk $SnO_2$ (JCPDS file No. 41-1445). The main strong peaks were observed at 26.02, 33.36, 37.8, 50.98 degrees assigned to (110), (101), (200) and (211) planes respectively. No other characteristic peaks can be observed. Such experimental results suggest that the products are of high crystalline and purity.

The morphologies and microstructures of the calcined products were illuminated by FESEM observations. The low-magnification FESEM image in Fig. 3a shows the as-sintered products. At the lower part, the dense film is composed of nanoparticles and the film thickness is 500-700 nm. The nanowires with an average length of 5-7 μm grow on the film. No other morphologies are observed.This indicates that the obtained product is of a high purity. The FESEM image in Fig. 3b confirms the detailed morphology of the nanowires root. The nanowires grow in criss-cross and the diameter is about 50-70 nm. The high-magnification FESEM in Fig. 3(c) shows clear cylindrical structures at the top end of the nanowire, and the diameter is approximately 25-35 nm.

The detailed structure of the nanowires array was investigated by using a transmission electron microscopy (TEM) and a high-resolution transmission electron microscopy (HRTEM) combined with the fast fourier transform (FFT) analysis. The typical TEM image in Fig. 4a shows. The results of the complete nanowire based on the FFT show that the nanowires from the USP products have two different crystal-lattice arrangements, as shown in Fig 4(b) and (c). The HRTEM images confirm the single-crystalline structures of the individual nanowires (fig. 4 (b1) and (c1)). The horizontal and vertical lattice fringe spacings were observed to be 3.34 ± 0.01 Å and 3.20 ± 0.01 Å, respectively. The FFT analytical results also confirm that they are in accordance with the (110) and (001) crystal face of anatase structures $SnO_2$. In Fig. 4 (c1), the lattice fringe spacings are 3.35 ± 0.01 Å and 2.65 ± 0.01 Å, and the growth direction is consistent with the [112] direction. The difference of the growth direction may be caused by oxygen defects on the surface of the $SnO_2$ nanoparticles which grow in the oxygen-deficient reaction zone. These defects can be observed in the HRTEM images. Such a result is similar to those of Zhang et al [19] and Xu et al [20].

To reveal the growth process and to explore the possible growth mechanism of $SnO_2$ nanowires, the study of the morphology evolution of $SnO_2$ with different reaction time has been conducted at 400 $^oC$ with a fixed precursor concentration (1 mol/L) and a carrier gas flow rate (500 sccm). The corresponding results are presented in Fig. 5. This figure shows that the non-uniform film consists of nanorods and island shape particles when the reaction lasts for 10 min. The length of nanowires is about 100-150 nm. In the latter stage of the USP (30 min, in Fig.5b), the film is entirely covered by island shape particles. The nanowires grow longer (300-500 nm), and scattered unequal. With the reaction carrying on (60 min), a uniform and compact film at the bottom was formed. The nanowires are of a 1 μm length and a 30-50 nm diameter with homogeneous micromorphology. After 2 hours of the USP, the nanowires significantly criss-cross grow, turned long and compactly cohered. The average length is 5-7 μm.

We propose the growth process of nanowires from the SEM and TEM images. Atomizing particles are deposited on the surface of substrates and form seed layer. The $SnO_2$ nanoscale particles are distributed in the aerosol environment and deposited on the substrate gradually. The $SnO_2$ nanowires grow from the high-surface-energy surface of the island shape nanoparticles. With the reaction going on, the seed layer becomes thicker and the nanowires grow long and dense. The time of the USP progress affect the size and density of the nanowire arrays.

It was inferred that the $SnCl_4$ solution was dried up and yielded $Sn(OH)_4$ crystal upon hydrolysis. To imitate the progress of the USP progress, the precursor solution (1 mol/l $SnCl_4$) was evaporated to dryness in a water bath at 50 $^oC$, and dried-up materials were analyzed by the TG–DSC (thermogravimetry-differential scanning calorimetry). Therefore, commercial $SnCl_4.5H_2O$ and $Sn(OH)_4$ were analyzed by the TG-DSC as references (curves (S2) and (S3)). The TG curves in Fig. 6 show four sections of mass losses, 16.8% (RT-200), 13.1% (200-350), and 6.7% (350-590)，while the no mass loss appears over 600 $^oC$ in the fourth section. The characteristic endothermic peaks emerge at 175 $^oC$, 300 $^oC$, and 515 $^oC$. The TG curve of $Sn(OH)_4$ in Fig. S3 reveals that the mass loss is about 18% in the section from 30 $^oC$ to 600 $^oC$. The characteristic endothermic peaks occur at 138 $^oC$，350 $^oC$, and 520 $^oC$. Crystal water was removed from hydration hydrogen tin oxide when the temperature rises to 138 $^oC$. When heated to 350 $^oC$, the $Sn(OH)_4$ decomposes into $SnO_2$ and water until the temperature reached 520 $^oC$. The TG curve of $SnCl_4.5H_2O$ in Fig. S4 shows that total mass reduces to 0% when the temperature rises from 30 $^oC$ to 190 $^oC$. The characteristic endothermic peaks appear at 74 $^oC$ and 190 $^oC$. At 74 $^oC$ the endothermic peak shows that the waterofcoordination and water of crystallization in the $SnCl_4.5H_2O$ were separated . The gasification of $SnCl_4$ absorbs heat at 190 $^oC$ with suddenly decreasing mass.

The morphology changes with various substrate temperatures are shown in Fig 7.(a-d). When the temperature was controlled below 150 $^oC$, liquid precursors directly reached the substrate and the products were globular. When the temperature reached about 300 $^oC$, the solution was dried. The amount of $SnCl_4$ $5H_2O$ reduced, and the precursor ($Sn(OH)_4$) began to break down to form $SnO_2$ crystal nucleus on the surface of substrate. With increasing temperature (400 $^oC$), $SnO_2$ nucleated and crystally grew. It thermally decomposed on the surface of the substrate and produced nanowires. At higher temperature (600 $^oC$), most precursors were broke down before they reached the substrate and formed $SnO_2$ particles, which were directly deposited onto the substrate and destroyed nanowires structures. The deposited film was formed by micro-particles instead of nanowires.

According to Fig. 6, Fig. S3 and Fig. S4, there is reason to suspect that precursor in reaction was composed of $SnCl_4$ and $Sn(OH)_4$. As the temperature increases, $SnCl_4$ is gradually vaporized. The amount of $SnCl_4$ takes part in the reaction to produce $SnO_2$ reduced. $Sn(OH)_4$ is mainly precursor to produce $SnO_2$ nanowires. Of all, temperature is a significant factor to decide the formation of nanowires. Under the proper temperature, $Sn(OH)_4$ (liquid) produces $SnO_2$ core as $SnO_2$ seed for it grows larger on the surface of substrates. It is the precondition of the preparation of nanomaterials with special morphology.

The proposed growth process of nanowires by the USP was divided into 6 phases (in Fig. 8). From Figs. 5-7, the growth progress and mechanism of nanowires prepared by the USP method were proposed as shown in Fig.8.

(1) Micrometer-sized $SnCl_4$ solution droplets isolated from others are obtained by high-intensity ultrasound.

(2) $SnCl_4$ solution droplets are hydrolyzed by the thermic effect and produce the mixture of $SnCl_4$-$5H_2O$ and $Sn(OH)_4$ (temp<150 $^oC$).

(3) $SnCl_4.5H_2O$ is absolutely evaporated to dryness besides liquid $Sn(OH)_4$. (150 $^oC$ <temp<300 $^oC$)

(4) Liquid $Sn(OH)_4$ gradually produces $SnO_2$ crystal nucleus. (300 $^oC$ <temp<350 $^oC$)

(5) The materials reached the quartz substrate which is the highest temperature section. Liquid $Sn(OH)_4$ is turned into islet-like $SnO_2$ particles. (temp>350 $^oC$)

(6) The prolysis of $Sn(OH)_4$ makes the $SnO_2$ seed layer particles on the quatz substrate. The small nanorods assemble by the nanoparticles.

(7) Nano-size $SnO_2$ particles are deposited on the quartz substrate continuously over time. Aerosol arrives at islet-like $SnO_2$ particles then oriented grows. At last, the $SnO_2$ nanowires are obtained. After they are sintered at 500 $^oC$, physical and chemical properties are improved.

The special morphology based on the $SnO_2$ nanowires may express better gas sensing properties than those of $SnO_2$ particles. Two sensors based on $SnO_2$ nanowires by the USP at 400 $^oC$ and nanoparticles sintered at 600 $^oC$ were tested at 150$^oC$, as shown in Fig.9a. Gas selectivities, especially for oxidizing gases: $O_3$, $SO_2$, $Cl_2$, $NO_2$ were investigated at 150$^oC$. They show that the sensing property of sensor based on $SnO_2$ nanowires is higher than $SnO_2$ particles. The response of the sensor based on $SnO_2$ nanowires to 2 ppm of $NO_2$ is as high as 6.9, and higher than other test gases. These $SnO_2$ nanowires allay materials turn out to possess fine sensing property to $NO_2$.

The responses of sensors using $SnO_2$ with different structures to various concentrations of $NO_2$ are compared in Fig.9b. The response of sensors based on $SnO_2$ particles to $NO_2$ almost do not change with increasing concentrations at 150$^oC$. The response to 10 ppm of $NO_2$ is 2.3. While the sensor based on $SnO_2$ nanowires expressed increases with increasing concentrations of $NO_2$, and the response to 10 ppm of $NO_2$ is as high as 21.1. This indicates its remarkable sensing property. The transient response and recovery characteristic to 2 ppm of $NO_2$ are illustrated in Fig.9c. When the sensor was exposed to $NO_2$ at 150$^oC$, resistance rises from 1.01 MΩ to 7 MΩ. The response and recovery time are 25 min and 45 min, respectively. Successive measurement show good repeatability.

The widely accepted gas sensing mechanism of metal-oxide semiconductor is based on the depletion layer model. When the materials are in the air, oxygen is adsorbed on the surface of $SnO_2$ nanowires, captured electron. Then depletion layer is formed. When they are exposed to oxidizing gas, competitive adsorption between oxidizing gas and oxygen occurred on the surface of the materials. The thickness of the depletion layer increases leading to the decrease of carriers. Hence, electrical conductivity decreased.

The correlative factors of the increased gas sensing properties of $SnO_2$ nanowires were analysed. During the progress of the USP and anneal, non-stoichiometric $SnO_2$ nanowires were produced in anoxic environments. To maintain the electrical neutrality, $Sn^{4+}$ gained electrons and turned to $Sn^{2+}$. For $SnO_2$ nanowires based sensors, oxygen vacancies ($V_o$• and $V_o$••) and mainly partially reduced cations $Sn^{2+}$ are the surface basic sites ($S_b$)s for $NO_2$ chemisorption[21-23]. The reaction at the surface basic sites is quite complex. The main reaction process is illustrated as follows.

$$NO_{2,gas} + Sn^{2+} \rightarrow (Sn^{3+} + NO_2^-{}_{,ads}) \quad (2)$$

or

$$NO_{2,gas} + e^- \rightarrow NO_2^-{}_{,ads} \quad (3)$$

At lower oxygen chemical potentials, oxygen depleted surface phases become energetically favored.

The vital factor to gas sensing properties of sensors based on $SnO_2$ nanowires is explained. First, there was large amount of oxygen defects on the surface of nanowires at room temperature. $NO_2$ can be selectively absorbed at the defect site and change the resistivity of the materials.

Second, the high surface to volume ratio of these nanostructures and excellent crystallinity enhanced contact area between sensing materials and gas atmosphere and provided highly reproducible transduction properties. Third, in contrast to the complex and random distribution of the inter grain barrier, resistance modulation in individual nanowires is straightforward. Nanowires have a larger contact area with gas, so they show a good response to $NO_2$ at room temperature.

**Conclusion**

In summary, high purity vertically aligned $SnO_2$ nanowire arrays were first prepared directly on a glass substrate via a ultrasonic spray pyrolysis method combined with sintering. The $SnO_2$ nanowire arrays consist of single crystalline nanowires with a diameter of 50-70 nm and a length of 5-7 μm. There were two different nanowire growth directions due to the oxygen defect growth. The gas sensing tests exhibit that the as-obtained $SnO_2$ nanowire arrays show better sensitivity, selectivity and stability to $NO_2$ than that based on $SnO_2$ nanoparticles. The promising gas sensing performance are owing to the oxygen defects in the nanowire arrays. The result demonstrates that the $SnO_2$ nanowire arrays can be used as a promising platform for sensing of $NO_2$.

## Acknowledgements:

This research was supported by the Youth academic elite funded projects of Harbin normal university, Science and technology research project of heilongjiang province department of education, China (NO.12541224,NO.12XQXG30). The project development plan of science and technology of Jilin Province (20130521009JH), National High-Tech Research and Development Program of China (863 Program, No. 2013AA030902, 2014AA06A505)

## References:

[1] ChePu Hsu, TsungWei Zeng, MingChung Wu, YuChieh Tu, HsuehChung Liao, WeiFang Su, Hybrid poly(3-hexyl thiophene)–$TiO_2$ nanorod oxygen sensor, RSC Adv., 2014,4, 22926-22930.

[2] DoHwan Nam, SungJin Lim, Min-Joong Kima, Hyuk-Sang Kwon, Facile synthesis of $SnO_2$-polypyrrole hybrid nanowires by cathodic electrodeposition and their application to Li-ion battery anodes, RSC Adv., 2013,3, 16102-16108.

[3] WeeJun Ong, Meei Mei Gui, Siang-Piao Chai, Abdul Rahman Mohamed, Direct growth of carbon nanotubes on Ni/$TiO_2$ as next generation catalysts for photoreduction of $CO_2$ to methane by water under visible light irradiation, RSC Adv., 2013,3, 4505-4509.

[4] Debin Kong, Haiyong He, Qi Song, Bin Wang, QuanHong Yang, Linjie Zhi, A novel $SnS_2$@graphene nanocable network for high-performance lithium storage, RSC Adv., 2014,4, 23372-23376.

[5] V. Anand Ganesh, Saman Safari Dinachali,Hemant Kumar Raut,Timothy Michael Walsh, A. Sreekumaran Nair, Seeram Ramakrishna, Electrospun $SiO_2$ nanofibers as a template to fabricate a robust and transparent superamphiphobic coating, RSC Adv., 2013,3, 3819-3824.

[6] Chuilin Lai, Xiaoxu Wang, Yong Zhao, Hao Fong, Zhengtao Zhu, Effects of humidity on the ultraviolet nanosensors of aligned electrospun ZnO nanofibers, RSC Adv., 2013,3, 6640-6645.

[7] Yulan Ren, Chunling Zhu, Shen Zhang, Chunyan Li, Yujin Chen , Peng Gao, Piaoping Yang,Qiuyun Ouyang,Three-dimensional $SiO_2$-$Fe_3O_4$ core/shell nanorod array/graphene architecture: synthesis and electromagnetic absorption properties,Nanoscale, 2013,5, 12296-12303

[8] Jesper Wallentin, Nicklas Anttu, Damir Asoli, Maria Huffman, Ingvar Aberg, Martin H.

Magnusson, Gerald Siefer, Peter Fuss Kailuweit, Frank Dimroth, Bernd Witzigmann, H. Q. Xu, Lars Samuelson, Knut Deppert, Magnus T. Borgstrom,InP Nanowire Array Solar Cells Achieving 13.8% Efficiency by Exceeding the Ray Optics Limit,Science,339,1057-1060.

[9] V.Cosovic, A.Cosovic, N.Talijan, D.Zivkovic, D.Manasijevic, Dusko Minic, Improving dispersion of $SnO_2$ nanoparticles in Ag-$SnO_2$ electrical contact materials using template method, Journal of Alloys and Compounds, 2013, 567, 33–39.

[10] Hongbin Feng, Jin Huang,Jinghong Li,A mechanical actuated $SnO_2$ nanowire for small molecules sensing,Chem. Commun., 2013,49, 1017-1019.

[11] Ritu Gupta,Giridhar U. Kulkarni,Holistic Method for Evaluating Large Area Transparent Conducting Electrodes,ACS Appl. Mater. Interfaces, 2013,5,730–736.

[12] Zh.D.Li,Y.Zhou,J.Ch.Song,T.Yu,J.G.Liu,Zh.G,Zou,Versatile nanobead-scaffolded N-$SnO_2$ mesoporous microspheres: one-step synthesis and superb performance in dye-sensitized solar cell, gas sensor, and photocatalytic degradation of dye,J. Mater. Chem. A, 2013,1, 524-531.

[13]Sunghoon Park, Hyunsung Ko, Soyeon An, Chongmu Lee, One-step synthesis of $SnO_2$-core/$Ga_2O_3$-shell nanowires by thermal evaporation,Materials Letters,2013,94,30–33.

[14]A. A. Zhukova, A. N. Shatokhin, F. N. Putilin, I. A. Petukhov, M. N. Rumyantseva, A. M. Gaskov,Effect of surface modification with palladium on the CO sensing properties of antimony-doped $SnO_2$ whiskers,Inorganic Materials,2013, 49,1005-1010 .

[15]Mutong Niu, Feng Huang, Lifeng Cui, Ping Huang, Yunlong Yu, Yuansheng Wang, Hydrothermal Synthesis, Structural Characteristics, and Enhanced Photocatalysis of $SnO_2$/α-$Fe_2O_3$ Semiconductor Nanoheterostructures,ACS Nano, 2010,4,681–688.

[16]Ying Liu, Erik Koep,Meilin Liu,A Highly Sensitive and Fast-Responding $SnO_2$ Sensor Fabricated by Combustion Chemical Vapor Deposition.Chem. Mater., 2005, 17,3997–4000.

[17]Zhaoyang Liu,Darren Delai Sun,Peng Guo ,James O. Leckie,An Efficient Bicomponent $TiO_2$/$SnO_2$ Nanofiber Photocatalyst Fabricated by Electrospinning with a Side-by-Side Dual Spinneret Method,Nano Lett., 2007,7,1081–1085.

[18]Junghwan Huh, Min-Kyu Joo, Doyoung Jang, Jong-Heun Lee,Gyu Tae Kim ,Reduced charge fluctuations in individual $SnO_2$ nanowires by suppressed surface reactions,J. Mater. Chem., 2012,22, 24012-24016.

[19]D.F.Zhang, L.D.Sun, J.L.Yin,C.H.Yan,Low-Temperature Fabrication of Highly Crystalline SnO2 Nanorods,Advanced Materials,2003,15,1022-1025.

[20]Xiangxing Xu, Jing Zhuang,Xun Wang, $SnO_2$ Quantum Dots and Quantum Wires: Controllable Synthesis, Self-Assembled 2D Architectures, and Gas-Sensing Properties,J. Am. Chem. Soc., 2008,130(37),12527–12535.

[21]Luca Francioso, Angiola Forleo, Simonetta Capone, Mauro Epifani, Antonella M. Taurino, Pietro Siciliano,Nanostructured $In_2O_3$-$SnO_2$ sol–gel thin film as material for $NO_2$ detection,Sensors and Actuators B,2006,114,646–655.

[22]Aleksander Gurlo,Nanosensors: towards morphological control of gas sensing activity. $SnO_2$, $In_2O_3$, ZnO and $WO_3$ case studies,Nanoscale, 2011,3,154-165.

[23]Francisco Hernandez Ramirez, Joan Daniel Prades, Albert Tarancon, Sven Barth, Olga Casals, Roman Jimenez Diaz, Eva Pellicer, Jordi Rodriguez, Joan Ramon Morante, Miguel Angel Juli, Sanjay Mathur,Albert Romano Rodriguez,Insight into the Role of Oxygen Diffusion in the Sensing Mechanisms of $SnO_2$ Nanowires,Adv. Funct. Mater. 2008, 18, 2990–2994

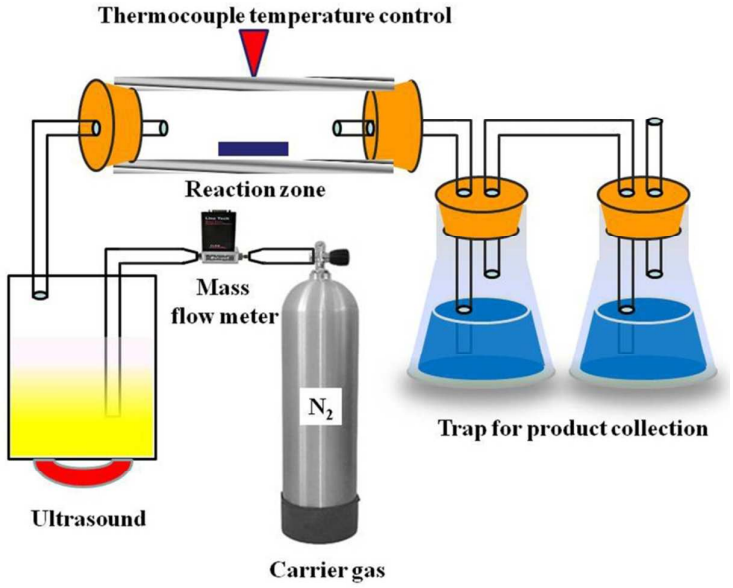


Figure 1 a) Schematic diagram of the ultrasonic spray pyrolysis system

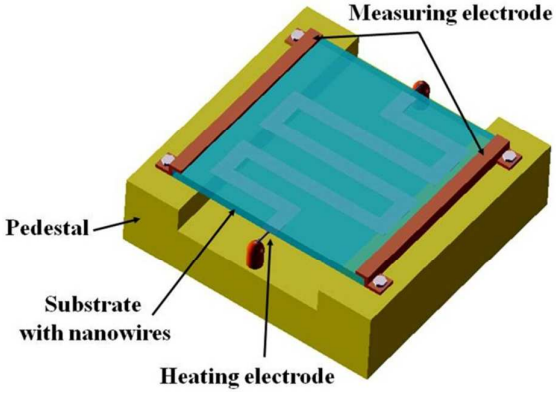


Figure 1 b). Structure schematic diagram of the device gas sensor

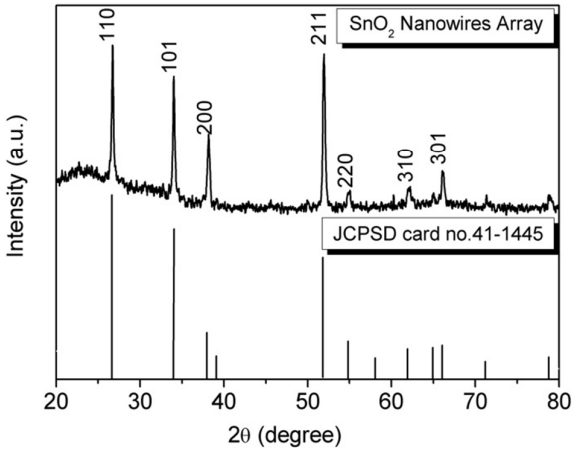


Figure 2. The X-ray diffraction results of the synthesized $SnO_2$ nanowires arrays.

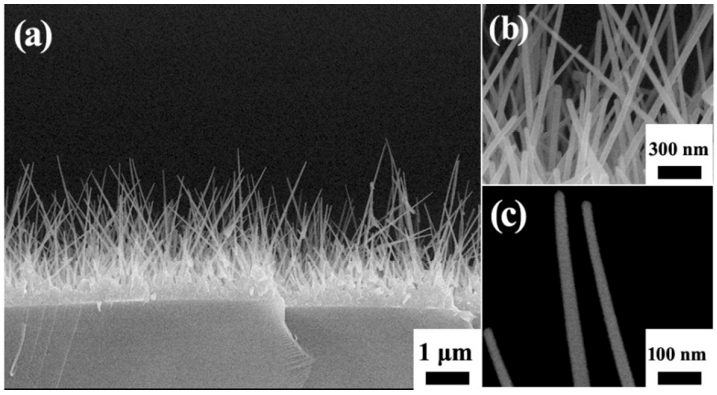


Figure 3. The morphologies and microstructures of the calcined products are illuminated by FESEM,a) The low-magnification FESEM image,b) and c) The high-magnification FESEM.

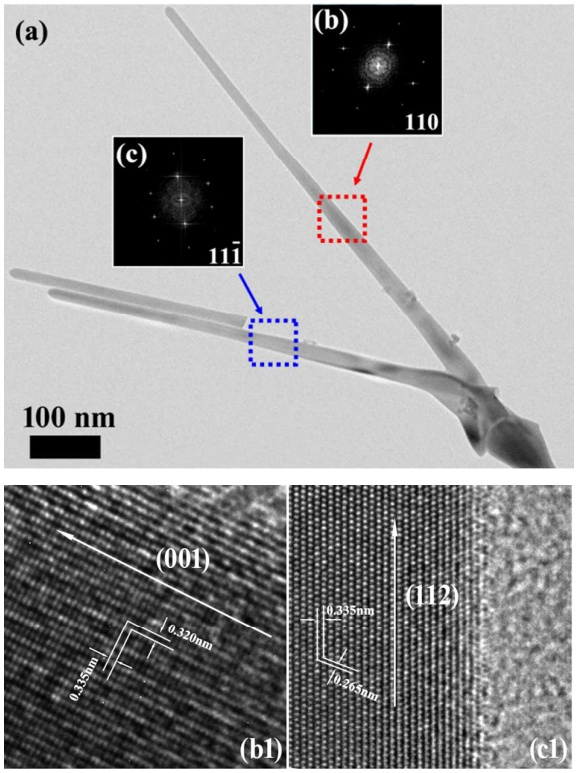


Figure 4.The detailed structures of the nanowires array with transmission electron microscopy (TEM) and high-resolution transmission electron microscopy (HRTEM) combined with fast fourier transform (FFT) analysis. a) The low-magnification TEM image, (b) and (c) nanowires of FFT from USP products have two different crystal-lattice arrangements, The HRTEM image nanowire (fig.4 (b1) and (c1))

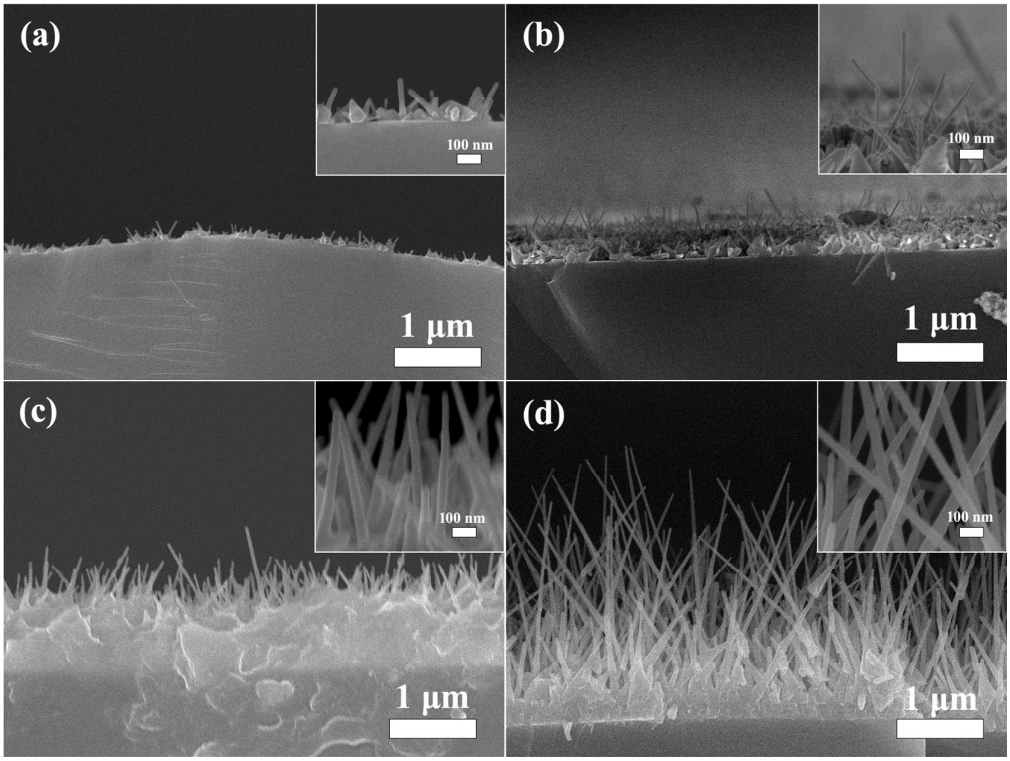


Figure 5.Nanowires growth process with the reaction time, a)10min, b)30min,c)60min,d)120min.

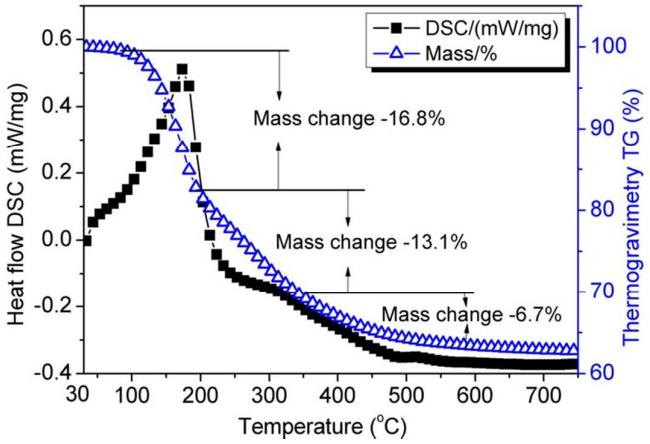


Figure 6. The TG–DSC (thermogravimetry–differential scanning calorimetry) results for the precursor.

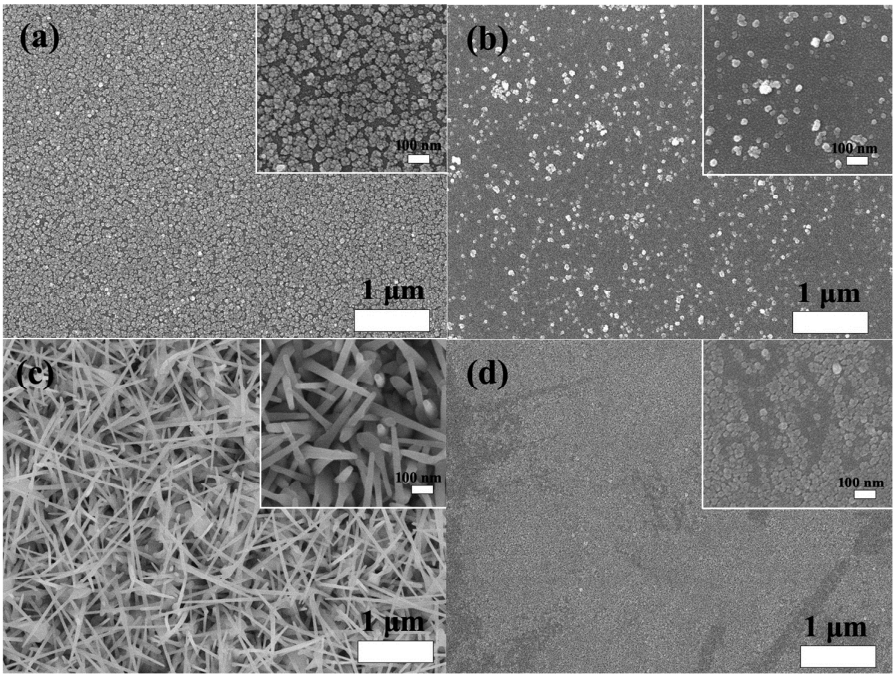


Figure 7.(a-d)The morphology changes with various substrate temperature, a) 150°C, b) 300 °C, c) 400 °C, d) 600 °C

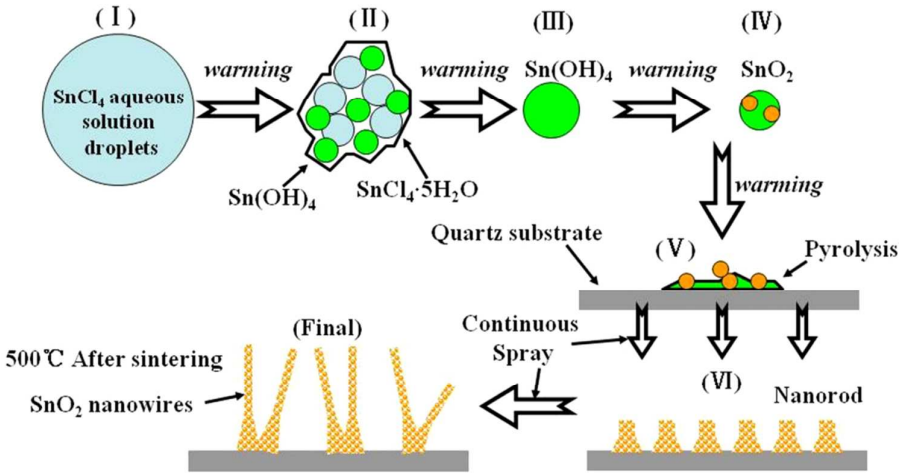


Figure 8. The proposed process of growth of nanowire by USP

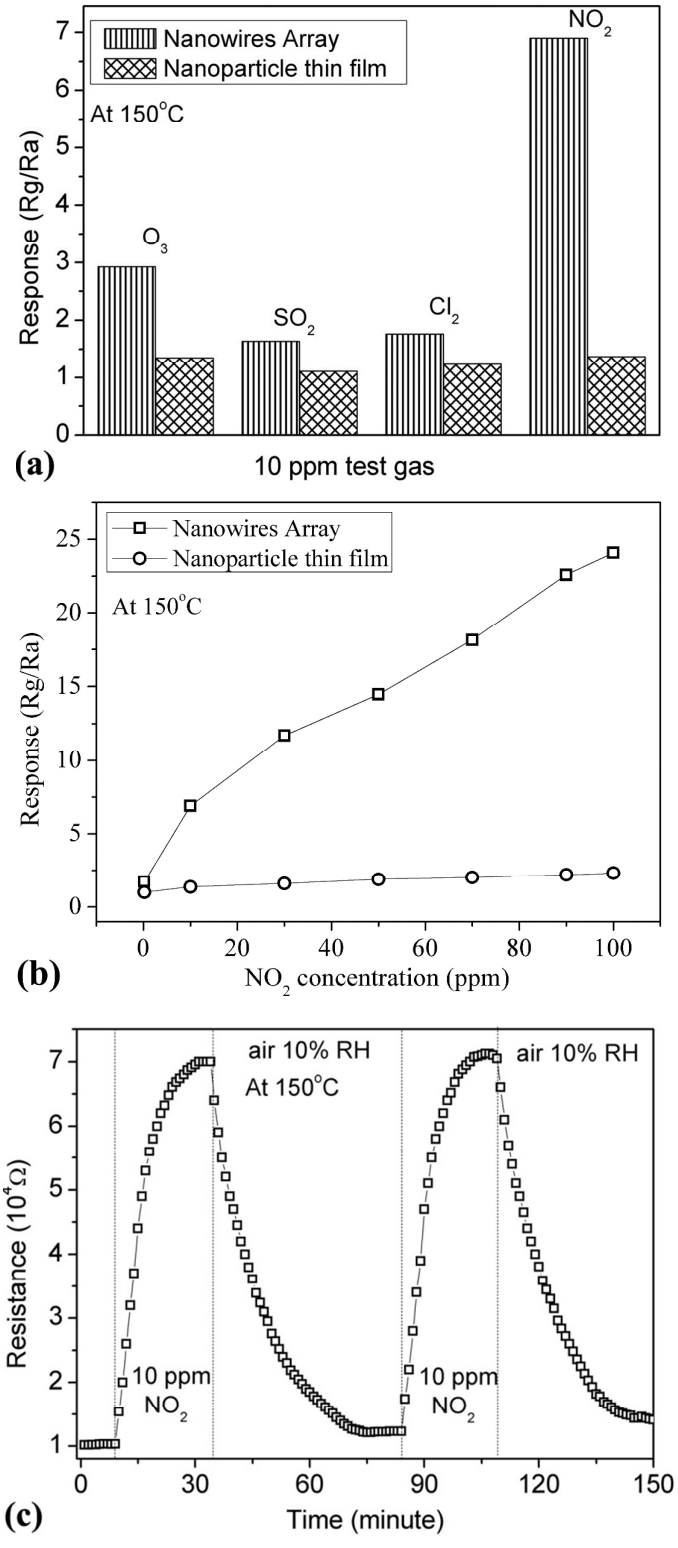


Figure.9 Gas sensitive performance test curves at 150°C. a) selectivity,b) concentrations,c) response and recovery.